Extension of Geldart's Diagram to Fluidizable Fine and Ultrafine Particles

Cite as: AIP Conference Proceedings **1145**, 977 (2009); https://doi.org/10.1063/1.3180094
Published Online: 01 July 2009

J. M. Valverde, and A. Castellanos

Extension of Geldart's Diagram to Fluidizable Fine and Ultrafine Particles

J. M. Valverde and A. Castellanos

Faculty of Physics. University of Seville. Avenida Reina Mercedes s/n, 41012 Seville. Spain.

Abstract. The Geldart's diagram, which was originally based on empirical observations on beds fluidized by air at ambient conditions, has been routinely used to predict the type of gas-fluidization expected for a granular material. However, the Geldart's diagram, based on particle size and density, is not currently a useful tool to predict the fluidization behaviour of many fine and ultrafine cohesive powders. There are recent reports revealing nonbubbling fluidlike fluidization for some preconditioned fine and ultrafine powders, in contrast with the predicted unfluidizable Geldart C behaviour according to their primary particle size. In this work we present an extension of Geldart's diagram that rationalizes the type of behaviour observed for this new class of fine and ultrafine powders. In our approach we have extended empirical criteria mostly used in the past to explain the behaviour of liquid-fluidized beds, showing that fluidization, either by liquid or gas, can be understood from a general frame. Our approach to treat gas-fluidized beds of fine cohesive particles considers particle agglomerates, grown to a size limited by the balance between interparticle force and flow shear, as effective low-density particles. In accordance with experimental observations, our diagram predicts that the nonbubbling fluidization regime can be just solidlike for slightly cohesive particles (Geldar A behaviour). When particle size is decreased, we predict the existence of a nonbubbling fluidlike regime for preconditioned powders as seen experimentally. For sufficiently small particles and/or high viscosity gases, the fluidized bed transits directly from the nonbubbling fluidlike regime to elutriation as observed in gas-fluidized beds of nanoparticles, fluidized beds of micrometric particles with high viscosity gas, and liquid-fluidized beds of moderate density large beads.

Keywords: Fluidized beds, Diffusion and aggregation, Granular flow
PACS: 47.55.Lm, 47.57.eb, 47.57.Gc

Fluidized beds are usually unstable and contain fluid bubbles arising through the bed which curtail uniform expansion and hamper the quality of fluid-solid mixing. The relative importance of interparticle forces and hydrodynamic forces on the distinction between nonbubbling and bubbling fluidization is still under debate [1, 2]. A relevant parameter that characterizes the cohesiveness of a granular material is the granular Bond number Bo_g, defined as the ratio of interparticle attractive force to particle weight. The attractive force F_0 between uncharged particles fluidized by dry gas arises mainly from the van der Waals interaction, $F_0 \simeq Ad_a/24z_0^2$, where $z_0 \simeq 3-4$ Å is the distance of closest approach between two molecules, A is the Hamaker constant, and d_a is the typical size of the surface asperities [3]. Typically $A \sim 10^{-19}$J and $d_a \sim 0.2\mu$m [3], which gives an estimate of $F_0 \sim 10$nN. In the case of noncohesive particles ($Bo_g < 1$, particle size $d_p > 100\mu$m) it is generally seen that gas-fluidized beds bubble just beyond the minimum fluidization point (Geldart B, bubbling powders [4]). For slightly cohesive beads ($Bo_g > 1$), gas-fluidized beds show a solidlike uniform fluidization interval, characterized by a stable expansion, and the fluidlike regime initiates just at the bubbling onset (Geldart A, aeratable powders [4]). Traditionally, cohesive particles ($Bo_g >> 1$, typically $d_p < 20\mu$m) have been impossible to fluidize uniformly by gas due to crack formations and channeling favored by strong cohesive forces (Geldart C, cohesive powders [4]). However it has been seen that some fine powders, with cohesion reduced by addition of surface additives, transit from the solidlike regime to a nonbubbling fluidlike one, and then to bubbling at higher gas velocities [5]. Let us call this novel transition SFB behavior (solidlike-to-fluidlike-to-bubbling). In this letter we map the fluidization behavior boundaries of cohesive powders from empirical relations well-known for liquid-fluidization of noncohesive particles that are modified to take into account aggregation in gas-fluidization of adhesive particles. We show the existence of a new gas-fluidization behavior, that we call SFE, in which the powder transits from solidlike to fluidlike to elutriation with full suppression of bubbling.

Harrison et al. [6] hypothesized that fluid bubbles in the fluidlike regime are no longer stable if their rising velocity U_b exceeds the terminal settling velocity of the individual particles $v_{p0} \simeq (1/18)(\rho_p - \rho_f)d_p^2 g/\mu$, where ρ_p is particle density, ρ_f is the fluid density, μ is the fluid viscosity, and g is gravitational acceleration. Using the semi-empirical relation $U_b \simeq 0.7\sqrt{gD}$, where D is the bubble size, we arrive then at $D_m/d_p \simeq (\rho_p - \rho_f)^2 g d_p^3/(13\mu)^2$ for the largest stable size of the bubbles D_m. Harrison et al. carried out an extensive se-

CP1145, *Powders and Grains 2009, Proceedings of the 6th International Conference on Micromechanics of Granular Media* edited by M. Nakagawa and S. Luding

ries of experimental observations on fluidized beds of noncohesive particles with varying μ, ρ_p and ρ_f and concluded that the ratio D_m/d_p coincided with bubbling behavior when $D_m/d_p > 10$, and with uniform fluidization when $D_m/d_p < 1$. The regime of behavior described approximately by $1 < D_m/d_p < 10$ defined a transition from nonbubbling to bubbling behavior. Following Wallis ideas, some authors [7] have suggested that stable bubbles in fluidized beds are an outcome of the formation of concentration shocks in particle concentration when the propagation velocity of a voidage disturbance u_ϕ surpasses the elastic wave velocity u_e of the bed. It is well accepted that u_ϕ can be derived from the relation $u_\phi = -\phi dv_g/d\phi$, where the gas velocity v_g is related to the particle volume fraction ϕ by the Richardson-Zaki equation $v_g = v_{p0}(1-\phi)^n$, being $n \simeq 5.6$ in the small Reynolds number limit. The elastic wave velocity u_e is given by $u_e = [(1/\rho_p)(\partial p/\partial\phi)]^{1/2}$ where p is the particle-phase pressure endowed by particle velocity fluctuations. There is not a general consensus on a correct formulation of $p(\phi)$ as recently discussed by Guazelli [8]. It is clear that p should increase with ϕ at low volume fractions, reach a maximum, and then decrease for larger ϕ [1], but a reliable equation for p is completely unknown. In our work we will use the equation $p \sim \rho_p g d_p \phi^2$, which is upheld by measurements of the collisional pressure in a water-fluidized bed [9], recent numerical studies [8], and the theoretical work by Batchelor [7] in the dilute limit. A similar relationship was also derived by Foscolo and Gibilaro [10]. Batchelor [7] pointed out however that this derivation was conceptually wrong, albeit Foscolo and Gibilaro found good agreement with observations on the initiation of visible bubbling under systematic variations of relevant parameters such as pressure, temperature and addition of fines [10].

Cohesive particles aggregate in a gas-fluidized bed driven by the dynamic equilibrium between interparticle attractive force F_0 and flow shear, which supports particles weight in the gravity field. Assuming that the maximum shear force that the aggregate in the fluidized bed can stand is of order of F_0, the scaling law $Bo_g \sim Nk^2 = k^{D+2}$ was derived to estimate the aggregate size d^* [2]. Here N is the number of particles aggregated, k is the ratio of d^* to particle size d_p, and $D = \ln N/\ln k$. If we consider aggregates as effective particles of density $\rho^* = \rho_p N/k^3$, the Harrison et al. modified equation that results from the balance between U_b and the settling velocity of an aggregate $v^* = v_{p0}N/k$ is thus

$$\frac{D_m}{d^*} \simeq \frac{1}{18^2\,0.7^2}\,\frac{\rho_p^2\, g\, d_p^3}{\mu^2}\, Bo_g^{(2D-3)/(D+2)} \qquad (1)$$

Analogously, and taking into account the volume fraction of the aggregates $\phi^* = \phi k^3/N$, we can write the modified Wallis criterion as

$$\begin{aligned} u_\phi^* &\simeq \phi\,\frac{1}{18}\,\frac{\rho_p\, g\, d_p^2}{\mu}\, n\left(1-\phi Bo_g^{(3-D)/(D+2)}\right)^{n-1} Bo_g^{2/(D+2)} \\ u_e^* &\simeq \left(g d_p \phi Bo_g^{(4-D)/(D+2)}\right)^{1/2} \\ u_\phi^* &= u_e^* \text{ at bubbling onset} \end{aligned} \qquad (2)$$

On the other side, the fluidlike regime is limited by jamming of the fluidized aggregates. At the fluid-to-solid transition these aggregates jam in a solidlike state with a particle volume fraction $\phi_J = \phi_J^* k^{D-3} \approx \phi_J^* Bo_g^{(D-3)/(D+2)}$, where ϕ_J^* is the volume fraction of the jammed aggregates. The bed will transit through the solidlike fluidization regime when $\phi < \phi_J$.

Let us denote by ϕ_b a solution of Eq. 2 in case it exists. If $\phi_b \geq \phi_s$, where $\phi_s > \phi_J$ is the particle volume fraction of the sample in its initial settled state, it is expected that the fluidized bed transits from the initial state to the bubbling regime as soon as v_g surpasses the minimum fluidization velocity (Geldart B behavior). If $\phi_b < \phi_s$, the system will exhibit an expanded nonbubbling fluidization regime. For $\phi_b < \phi_J$, the bed might even show a solidlike regime followed by fluidlike regime and a transition to bubbling at high gas velocities (SFB behavior). The existence of a nonbubbling fluidlike regime depends however on the necessary condition $D_m/d^* < 10$. Otherwise the stable fluid pockets reach a macroscopic size leading to bubbling just above the jamming transition (in that case we would have a transition from expanded solidlike to bubbling regime: Geldart A behavior). Using Eq. 1 in Eq. 2 it can be shown that $u_e^* - u_\phi^* = u_e^*[1 - 0.7n(D_m/d^*)^{1/2}(\phi^*)^{1/2}(1-\phi^*)^{n-1}]$. Since $(\phi^*)^{1/2}(1-\phi^*)^{n-1}$ takes a maximum value of 0.195 at $\phi^* = 0.098$, we have that $\min(u_e^* - u_\phi^*) > 0$ for $D_m/d^* < 1.72$. Thus for $D_m/d^* < 1.72$ it is $u_e^* > u_\phi^*$ $\forall\phi > 0$, indicating that the system will transit from the solidlike regime to a fluidlike regime and from the fluidlike regime to elutriation (SFE behavior) with full suppression of bubbling. To our knowledge this is the first time that a direct agreement between the Harrison et al. and Wallis criteria is analytically established.

In Fig. 1 we plot ϕ_b, ϕ_J and D_m/d^* vs. d_p using $\rho_p = 1135\text{kg/m}^3$, $\mu = 1.79\times10^{-5}$Pa s, $F_0 = 2$nN, $\phi_J^* = 0.51$, and $D = 2.5$. These values correspond to fluidization of Xerox toners (polymer particles coated with silica nanoparticles) by dry nitrogen at ambient conditions [2]. Surface coating with silica nanoparticles decrease the typical surface asperity size down to the size of nanoparticle aggregates on the particle surface (of size around 50nm [2]) and thus decrease F_0 [2]. Data of ϕ_J and ϕ_b from experiments on Xerox toners (see ref. [2] for experimental details) have been plotted, showing good agree-

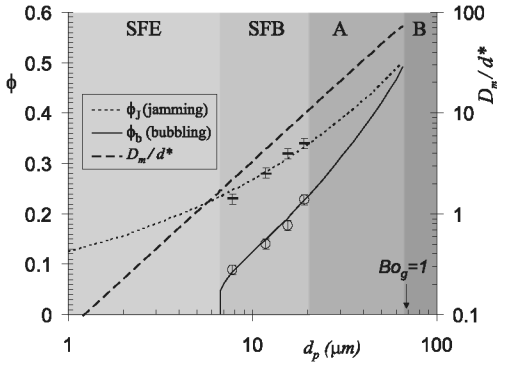

FIGURE 1. Phase diagram determining the transition between fluidization behaviors as a function of particle size. Left axis: particle volume fraction at the jamming transition ϕ_J and at the transition to bubbling ϕ_b. Right axis: Ratio of the maximum stable size of a fluid pocket to particle size in the fluidlike regime. $\rho_p = 1135\text{kg/m}^3$, $\rho_f = 1\text{kg/m}^3$, $\mu = 1.79 \times 10^{-5}$Pa s, $F_0 = 2\text{nN}$, $g = 9.81\text{m/s}^2$, $\phi_J^* = 0.51$, and $D = 2.5$. Experimental data on the jamming and bubbling transitions for fluidized beds of Xerox toners [2] are shown.

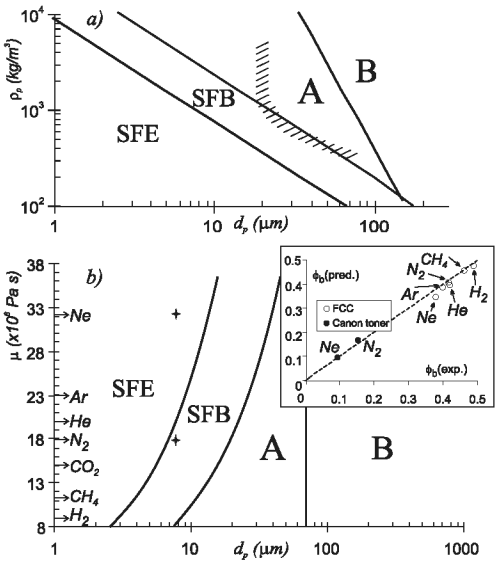

FIGURE 2. Effect of particle density (a) and gas viscosity (b) on the boundaries between types of fluidization shown in Fig. 1. The shaded line represents the boundary between A and C powders as shown in the original Geldart diagram [4]. The inset of (b) shows the particle volume fraction predicted vs. experimentally measured at bubbling onset for FCC (A behavior) and Canon toner (SFB behavior) powders fluidized with different gases (indicated) at ambient conditions.

ment with the expected values. We predict Geldart B behavior for $d_p > 70\mu$m, Geldart A behavior for $20\mu\text{m} < d_p < 70\mu$m, SFB behavior for $6.7\mu\text{m} < d_p < 20\mu$m, and SFE behavior for $d_p < 6.7\mu$m. Remarkably the A-B boundary coincides with $Bo_g \simeq 1$, which is also the limiting condition for aggregation. The criterion $Bo_g \simeq 1$ for the A-B boundary was already derived by Molerus [11] from analysis of experimental data and by Rhodes et al. [12] using Discrete Element Modeling. However the A-B boundary cannot be sharply defined since the existence of nonbubbling expansion beyond minimum fluidization depends on the history of the sample. For noncohesive hard spheres settled in the gravity field ϕ_s only varies slightly between 0.6 (random loose packing) and 0.64 (random close packing). Thus near $Bo_g \simeq 1$ bed expansion is difficult to measure and usually depends on experimental details as for example heterogeneous distribution of gas flow due to nonuniform porous distributor plate. This is illustrated in the work by Loezos et al. [1], who observed the fluidization behavior of glass beads ($\rho_p \simeq 2500\text{kg/m}^3$) in the size range $60\mu\text{m} < d_p < 200\mu$m. They observed that for $d_p < 100\mu$m the bed maintained a solidlike smooth appearance with no sustained bubbling (Geldart A behavior). For $d_p > 100\mu$m the window of stable expansion was very small, which was consistent with Geldart B behavior. However occasional bubbles could be observed near the top free surface for 88μm sized beads when the gas velocity was only slightly larger than the minimum fluidization velocity. Interestingly the limit $Bo_g \simeq 1$ for this material (using $A \simeq 1.5 \times 10^{-19}$J for glass and $d_a = 0.2\mu$m) is found for $d_p \simeq 90\mu$m. We must note that the parameters used to plot the type of diagram in Fig. 1 depend on each particular system. Particularly ϕ_J^* increases as F_0 is decreased or ρ_p increased [2], but the condition $Bo_g \simeq 1$ for the A-B boundary is independent on the value of ϕ_J^*. On the other hand, aggregates are composed of just a few particles for slightly cohesive powders and cannot be strictly considered as fractals. However in this limit the value of D does not play a relevant role and similar results are obtained using the equations for nonagglomerated particles.

In Fig. 2a we show the effect of particle density ρ_p on the gas-fluidization behavior. We show also the boundary drawn by Geldart [4] to separate empirically cohesive C powders and aeratable A powders. Interestingly the SFB-A boundary matches the Geldart C-A boundary for moderate values of particle density. It must be remarked however that the original Geldart diagram was derived from experiments on history-dependent samples, typically cohesive powders for which fluidization was not preceded by a pre-conditioned procedure. Convenient initialization facilitates fluidization by breaking contacts down to the level of primary particles, thus erasing powder memory and allowing individual particles to aggregate in fractal agglomerates. Interparticle adhesive forces are largely increased by stresses applied during powder history [2] and, as a consequence, large coherent fragments of the consolidated powder are difficult to break by the gas, giving raise the classical Geldart C behavior char-

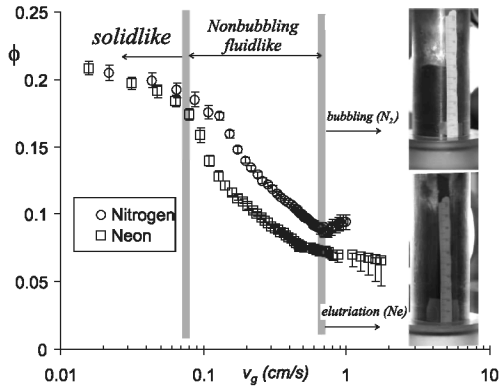

FIGURE 3. Particle volume fraction measured vs. gas velocity in fluidized beds of toner ($\rho_p = 1135\text{kg/m}^3$, $d_p = 7.8\mu\text{m}$) with N_2 and Ne at ambient conditions. Fluidization regimes are delineated. Inset: photographs of the fluidized bed in the bubbling regime (top) and elutriation regime (bottom).

acterized by strongly heterogeneous fluidization (rising plugs, rat holes, channeling, etc.). This memory effect is minimized by coating the particles with surface additives. Fluidization can be made also possible by vibration, placing magnetic beads within the powder that are agitated by an oscillating magnetic field, centrifugation or by means of sound wave excitation at low frequencies. Our diagram predicts which type of fluidization is to be expected for pre-conditioned cohesive powders. For example, when silica nanoparticles ($d_p = 12\text{nm}$, $\rho_p = 2560\text{kg/m}^3$) are fluidized with nitrogen, SFE behavior is seen [14], whereas SFB behavior is observed for fluidization of titania nanoparticles ($d_p = 21\text{nm}$, $\rho_p = 4500\text{kg/m}^3$). The study of nanopowders requires however further elaboration since for these samples the effective primary particles in fluidization are pre-existing simple-agglomerates [15]. The typical density and size of these simple-agglomerates for silica nanopowder are $\rho_s \approx 50\text{kg/m}^3$ and $d_s \approx 30\mu\text{m}$ [14, 15], which according to Fig. 2a would give SFE behavior in agreement with experimental observations. For titania nanopowder simple-agglomerates are denser ($\rho_s \approx 100\text{kg/m}^3$) [14], which shifts the fluidization behavior to SFB as seen experimentally [14].

The effect of fluid viscosity on the fluidization behavior boundaries is shown in Fig. 2b. Accordingly, it has been observed that Geldart A powders at ambient conditions can be uniformly fluidized with substantial expansion under conditions at elevated temperature [10]. Likewise improvement of fluidization quality and enhanced fluidlike expansion have been reported when high viscosity gases are used [3]. The inset of Fig. 2b shows good agreement between the values of ϕ_b predicted and the measured for two different cohesive powders fluidized with different gases, Geldart A FCC catalyst ($\rho_p \simeq 887\text{kg/m}^3$, $d_p \simeq 59.4\mu\text{m}$) [3], and Canon CLC700 toner ($\rho_p \simeq 1200\text{kg/m}^3$, $d_p \simeq 8.5\mu\text{m}$, $F_0 \simeq 10\text{nN}$) exhibiting SFB behavior (see ref. [2] for experimental details). Figure 2b predicts that a $7.8\mu\text{m}$ particle sized Xerox toner ($\rho_p \simeq 1135\text{kg/m}^3$, $F_0 \simeq 2\text{nN}$) showing SFB behavior when fluidized with nitrogen would shift its behavior to SFE when fluidized with neon (see symbols in main graph). In Fig. 3 we plot experimental data of ϕ vs. gas velocity v_g. The fluidized bed consists of a vertical 4.42cm dia. vessel containing the powder which is subjected to a controlled flow of gas injected through a gas distributor at its bottom. ϕ is derived from the height of the bed, which is measured by an ultrasonic sensor placed on top of the vessel. It is seen that the type of gas does not play a major role on bed expansion in the solidlike regime since the hydrodynamic interaction is not relevant. On the other hand the bed expands to smaller values of ϕ for neon in the fluidlike regime. In agreement with our prediction the bed fluidized with nitrogen transits to bubbling and the one fluidized with neon transits to elutriation. In the former case ϕ reaches a minimum at the bubbling transition, characterized by oscillations of the bed height due to bubbles burst on the free surface, and the elutriated mass of powder is small. In the latter the height of the diffused free surface and the mass of elutriated powder increase monotonically as the gas velocity is increased.

ACKNOWLEDGMENTS

We acknowledge Spanish Government Agency Ministerio de Ciencia y Tecnologia (contract FIS2006-03645) and Junta de Andalucia (contract FQM 421).

REFERENCES

1. S. Sundaresan, Annu. Rev. Fluid Mech. **35**, 63 (2003).
2. A. Castellanos, Adv. Phys. **54**, 263 (2005).
3. K. Rietema, *The Dynamics of Fine Powders* (Elsevier, London 1991).
4. D. Geldart, Powder Technol. **7**, 285 (1973).
5. J.M. Valverde et al., Phys. Rev. Lett. **86**, 3020 (2001).
6. D. Harrison et al., Trans. Inst. Chem Eng. **39**, 202 (1961).
7. G. K. Batchelor, J. Fluid Mech. **193**, 75 (1988).
8. E. Guazzelli, in *The Physics of Granular Media*, p. 213 (Wiley-VCH, Germany 2004).
9. R. Zenit et al., J. Fluid Mech. **353**, 261 (1997).
10. S. Rapagna, P.U. Foscolo, and L.G. Gibilaro, Int. J. Multiphase Flow **20**, 305 (1994).
11. O. Molerus, Powder Tech. **33**, 81 (1982).
12. M.J. Rhodes et al., Chem. Engng. Sci. **56**, 69 (2001).
13. R. Pfeffer et al. US2006086834 patent.
14. C. Zhu et al., AIChE J. **51**, 426 (2005).
15. J. M. Valverde and A. Castellanos, AIChE J. **52**, 838 (2006).